Ore Geology Reviews 86 (2017) 426–439

Contents lists available at ScienceDirect

Ore Geology Reviews

journal homepage: www.elsevier.com/locate/oregeo

LA-ICP-MS trace element geochemistry of garnets: Constraints on hydrothermal fluid evolution and genesis of the Xinqiao Cu–S–Fe–Au deposit, eastern China

Yu Zhang [a,b,c], Yong-jun Shao [b,c,*], Cheng-dong Wu [d], Hua-yong Chen [a,e]

[a] Key Laboratory of Mineralogy and Metallogeny, Guangzhou Institute of Geochemistry, Chinese Academy of Sciences, Guangzhou 510640, China
[b] Key Laboratory of Metallogenic Prediction of Nonferrous Metals and Geological Environment Monitor (Central South University), Ministry of Education, Changsha 410083, China
[c] School of Geosciences and Info-Physics, Central South University, Changsha 410083, China
[d] 304 Brigade of Hunan Nuclear Geology, Changsha 410000, China
[e] Guangdong Provincial Key Laboratory of Mineral Physics and Materials, Guangzhou 510640, China

ARTICLE INFO

Article history:
Received 26 November 2016
Received in revised form 3 March 2017
Accepted 6 March 2017
Available online 7 March 2017

Keywords:
Xinqiao Cu–S–Fe–Au deposit
Garnet trace element geochemistry
Stratiform mineralization
Middle-Lower Yangtze River Valley metallogenic belt
Eastern China

ABSTRACT

The Xinqiao Cu–S–Fe–Au deposit in the Tongling ore district, an important part of the Middle-Lower Yangtze River Valley metallogenic belt in eastern China, is located along the northern margin of the Yangtze Block. The deposit consists of two major mineralization types: stratiform and skarn (the genesis of the former is disputed). The more important stratiform orebody (90% of the total Cu, S and Fe reserves) has abundant garnet as the main gangue mineral, similar to the skarn orebody hosted in the intrusive contact.

Garnets from the Xinqiao stratiform orebody range from pure andradite (And_{100}) to $And_{50}Gro_{46}$, and can be divided into the early (Grt1) and late (Grt2) generation. Both generations contain low MnO (0.19–0.89%), wide range of Y/Ho (39.0–40.7 for Grt1, 29.8–67.9 for Grt2), and do not contain melt or fluid-melt inclusions, indicative of a magmatic-hydrothermal replacement origin. Grt1 and the Grt2 cores are grandite, whilst the Grt2 rims are mainly andradite with some grandite zones. Grandite is enriched in heavy rare earth elements (HREEs), and displays low ΣLREE/ΣHREE, La_N/Yb_N and U concentrations with negative Eu anomalies, whereas andradite is HREE-depleted, and displays high ΣLREE/ΣHREE, La_N/Yb_N ratios and U concentrations with positive Eu anomalies. The distinct trace element features suggest that the hydrothermal fluids for Grt1 and the Grt2 cores were of nearly neutral (pH), relatively oxidized and HREE-enriched, whereas those for the Grt2 rims had experienced episodic inflections between a mildly acidic, relatively reduced and HREE-depleted fluid and a nearly neutral, relatively oxidized and HREE-enriched fluid. Meanwhile, they also reveal that Grt1 and the Grt2 cores may have formed by diffusive metasomatism in a closed system, whereas the Grt2 rims may have formed by infiltration metasomatism in an open fracture system, possibly related to the unconformity that hosts the Xinqiao stratiform orebody. We propose that the Xinqiao stratiform orebody may have formed from Early Cretaceous magmatic-hydrothermal fluids associated with the Jitou stock, similar to the skarn-type orebodies in the district.

1. Introduction

Skarn deposits represent a globally important source of Cu, Fe, Pb, Zn, W, Ag, and Au. Skarn-related garnets could be formed by both contact metamorphism and hydrothermal alteration of carbonate-bearing rocks. These garnets have commonly distinct oscillatory chemical zonation, which can reflect the fluid-rock interaction history and provide a continuous physicochemical record of the hydrothermal evolution (Yardley et al., 1991; Jamtveit et al., 1993; Crowe et al., 2001; Fernando et al., 2003; Smith et al., 2004; Kim, 2006; Martin et al., 2011). Due to the recent development of electron probe microanalyzer (EPMA) and laser ablation inductively coupled plasma mass spectrometry (LA-ICP-MS) technology and the distinct garnet geochemistry (e.g., high Lu/Hf and Sm/Nd and ability to fractionate HREEs) (Scherer et al., 2000; Pertermann et al., 2004; Gaspar et al., 2008;

* Corresponding author at: Key Laboratory of Metallogenic Prediction of Nonferrous Metals and Geological Environment Monitor (Central South University), Ministry of Education, Changsha 410083, China.
E-mail address: shaoyongjun@126.com (Y.-j. Shao).

http://dx.doi.org/10.1016/j.oregeorev.2017.03.005
0169-1368/

Schmidt et al., 2011; Cheng et al., 2012), garnet has been widely applied to study the hydrothermal fluid evolution of skarn deposits (Jamtveit et al., 1993; Smith et al., 2004; Somarin, 2004; Gaspar et al., 2008). However, these garnets are typically Al-rich (e.g., pyrope, almandine, spessartine and grossular) and little attention was paid to the Fe-rich members (e.g., andradite), which are also common in many skarn systems (Gaspar et al., 2008; Zhai et al., 2014).

The Tongling ore district in the Middle-Lower Yangtze River Valley metallogenic belt in Eastern China, is located along the northern margin of the Yangtze craton (Fig. 1). It is well-known in China to have widespread Yanshanian granitoids and host numerous skarn type deposits (Mao et al., 2011), such as Tongguanshan, Fenghuanshan and Shizishan Cu deposits. However, the discovery of the large-scale stratiform orebodies in the Xinqiao Cu–S–Fe–Au deposit and the Dongguashan Cu–Au deposit (Fig. 2) has added extra complexities to the regional metallogenesis. The genesis of these stratiform orebodies has been controversial over the past forty years, and is variably argued to be sourced from: 1) Late Paleozoic (Hercynian) submarine exhalative processes (Fu et al., 1977; Xu and Zhu, 1978; Gu and Xu, 1986; Gu et al., 2000; Xu and Zhou, 2001; Xu et al., 2004); 2) Early Cretaceous (Yanshanian) magmatic-hydrothermal fluids (Chang and Liu, 1983; Chang et al., 1991; Zhai et al., 1992; Meng, 1994, 1996; Pan and Done, 1999; Mao et al., 2009, 2011) and 3) Yanshanian magmatism overprinting on Hercynian submarine exhalative processes (Yang et al., 1982; Xie et al., 1995; Tang et al., 1998; Zhou et al., 2010; Guo et al., 2011). It is confirmed that there is extensive skarn alteration in these stratiform orebodies (Chang and Liu, 1983; Chang et al., 1991; Zhang et al., 2016). However, skarn minerals (e.g., garnet, epidote) can form via not only magmatic hydrothermal replacement but also magmatism, submarine sedimentary exhalative processes and regional metamorphism (Einaudi and Burt, 1982; Doyle and Allen, 2003; Meinert et al., 2005). Previous studies paid little attention to the skarn minerals from Dongguashan and Xinqiao stratiform orebodies except for few garnet microthermometry research (i.e., Huang et al., 2003; Zhang, 2015), and it is unclear whether there were the skarn minerals related to the submarine sedimentary exhalative processes in the stratiform orebodies, corresponding to the last two hypotheses. Therefore, the generation and the origin of the Dongguashan and Xinqiao skarn minerals need further investigation to constrain on the stratiform orebody genesis.

This study focuses on the Xinqiao Cu–S–Fe–Au deposit (0.5 Mt Cu @ 0.71%, 75.5 Mt of sulfur @ 29.3%, 24.9 Mt Fe @ 46%, 11.2 t Au @ 4.7 g/t and 248.4 t Ag @ 248.4 g/t; Xu and Zhou, 2001), one of the largest deposits in the Tongling ore district (Fig. 1), as an example with the aim of tackling the above-mentioned issues from a garnet geochemical perspective. We report new field geological, mineralogical and EPMA and LA-ICP-MS garnet geochemical data from the Xinqiao stratiform orebody, and then discuss the geochemical characteristics of the Xinqiao garnet, and their implications on the garnet formation, hydrothermal fluid evolution and Cu–S–Fe–Au mineralization.

2. Geological setting

2.1. Regional geology

The Yangtze block is separated from the North China Craton by the Triassic Dabie orogenic belt to the north, and from the Cathaysian block by the Neoproterozoic suture to the south (Fig. 1; Li et al., 2014). The Middle-Lower Yangtze River Valley metallogenic belt is located in the Yangtze block and is well known for its abundant (more than 200) polymetallic deposits (Ling et al., 2009). The Tongling ore district, located in the central part of the Middle-Lower Yangtze River Valley metallogenic belt (Fig. 1), is the largest Cu–Au–Fe–Mo ore district in the belt and hosts numerous skarn deposits (Tang et al., 1998; Pan and Done, 1999; Lai and Chi, 2007; Mao et al., 2011). More than 50 ore deposits have been discovered in the Tongling district (Wu et al., 2014), and they are clustered in five orefields distributed from east to west, namely Tongguanshan, Shizishan, Xinqiao, Fenghuangshan and Shatanjiao, respectively (Fig. 2). The dominant lithologies in the Tongling district are marine and continental sedimentary rocks. Marine sedimentary rocks including clastic sedimentary rocks, carbonates, and evaporites, were deposited in the Silurian – Middle Triassic,

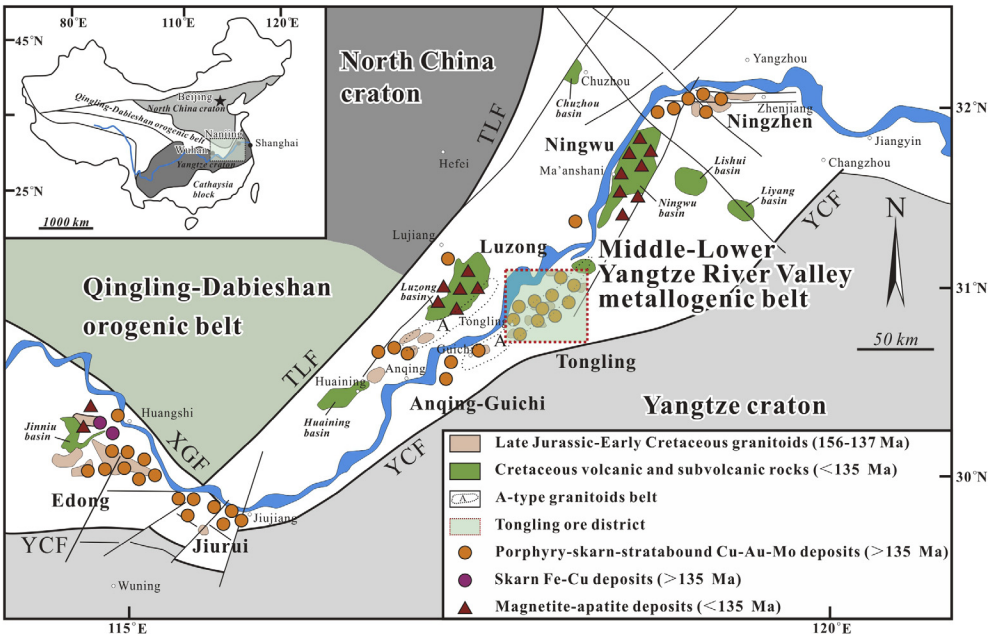

Fig. 1. Location of the Tongling ore district in the Middle-Lower Yangtze River Valley metallogenic belt (after Mao et al., 2011). TLF: Tancheng–Lujiang fault; XGF: Xiangfan–Guangji fault; YCF: Yangxing–Changzhou fault.

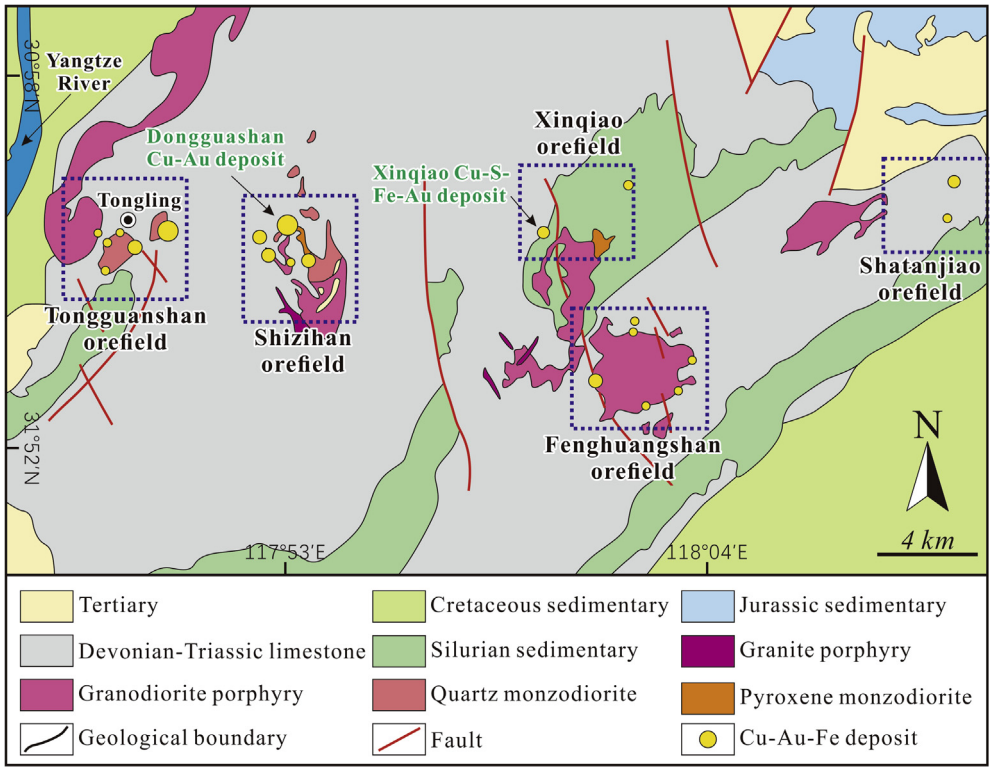

Fig. 2. Geological map of the Tongling district (modified from Chang et al., 1991).

with the exception of the Early – Middle Devonian. Continental rocks include clastic and volcanic-sedimentary rocks ranging from Middle Jurassic to Quaternary, excluding the Middle-Late Devonian (Wang et al., 2015; Cao et al., 2017). The sedimentary rocks are developed on a stable Precambrian basement, forming a thick sequence that became the country rocks for later Cu, Au, Fe, and Mo mineralization (Chang et al., 1991; Zhai et al., 1992; Cao et al., 2017). The Lower Permian Qixia Formation and the Lower Triassic Nanlinghu Formation are dominated by limestone and important ore-hosting rocks of the widespread skarn mineralization in this district, and the unconformity between the Upper Devonian Wutong Formation quartz sandstone and the Upper Carboniferous Huanglong Formation dolomite and limestone, constrains the economically significant stratiform mineralization in this district, such as the Xinqiao and Dongguashan deposits. Structurally, the region contains NE-trending folds and NNE- and NW-trending faults which control the intrusion emplacement. Igneous rocks are widely distributed in the region, including more than 70 intrusions and making up approximately 10% of the area, and are dominated by Late Jurassic – Early Cretaceous (ca. 156–137 Ma) high-K calc-alkaline intermediate granitoids (e.g., granite porphyry, granodiorite porphyry and quartz monzodiorite) (Fig. 2; Mao et al., 2011; Wang et al., 2015; Cao et al., 2017). Many small plutons with surface exposures from 0.15 to 5.00 km^2 occur as composite stocks, dikes and sills in this region (Du et al., 2015).

2.2. Ore deposit geology

The sedimentary rocks that crop out in the mining area range from the Middle-Upper Silurian sandstone and siltstone to the Lower Triassic Yinkeng Formation limestone, whereas Lower Carboniferous unit is absent. Major structures at Xinqiao are the NE-trending Dachengshan anticline and the NNE-trending Shenchong syncline, and the joint of the two folds is advantageous location of magmatic rocks and orebody (Fig. 3a). The dominant igneous rock in the region is the Jitou stock, which is a multiphase intrusion with quartz diorite at the center and diorite porphyry along the margin. The quartz diorite from Jitou stock was SHRIMP zircon U-Pb dated to be 140.4 ± 2.2 Ma (Early Cretaceous; Wang et al., 2004).

The two major mineralization types at Xinqiao include: the economically significant stratiform mineralization (accounting for 90% of the Cu, S and Fe reserves) confined along the unconformity between the Upper Devonian Wutong Formation quartz sandstone and the Upper Carboniferous Huanglong Formation limestone; and the economically less important skarn-type mineralization hosted along the intrusive contact between the Jitou stock and the Lower Permian Qixia Formation limestone (Fig. 3b).

The NW-dipping stratiform orebody is 2560 m long, 1810 m wide and on average 21 m thick (Fig. 3b), with a pyrite-bearing quartz stockwork in the Upper Devonian Wutong Formation, which is dominated by quartz sandstone and acts as the footwall of the stratiform orebody. Field geologic and petrographic observations indicate that ore minerals in the stratiform orebody include magnetite, chalcopyrite, pyrrhotite, hematite, native gold and electrum (Dai and Liu, 1984), whereas gangue minerals include primarily garnet, diopside, epidote, chlorite, quartz and calcite. Detailed field investigation indicates that the wallrock alteration of the stratiform orebody include garnet, sericite, quartz, chlorite and kaolinite, with silicic alteration developed in the footwall of the orebody.

As for the skarn-type orebody, both the endoskarn and exoskarn are calcic skarn, and consist predominately of garnet, wollastonite and subordinate pyroxene (Wang et al., 2011). Major metallic minerals include massive/vein/disseminated magnetite, pyrite, chalcopyrite, pyrrhotite, sphalerite and galena.

Zhang et al. (2016) argued that the stratiform mineralization may have been associated with the Jitou stock, as may also be the case for the skarn-type orebody. Based on mineral assemblages and textural relationships, these authors divided the Xinqiao

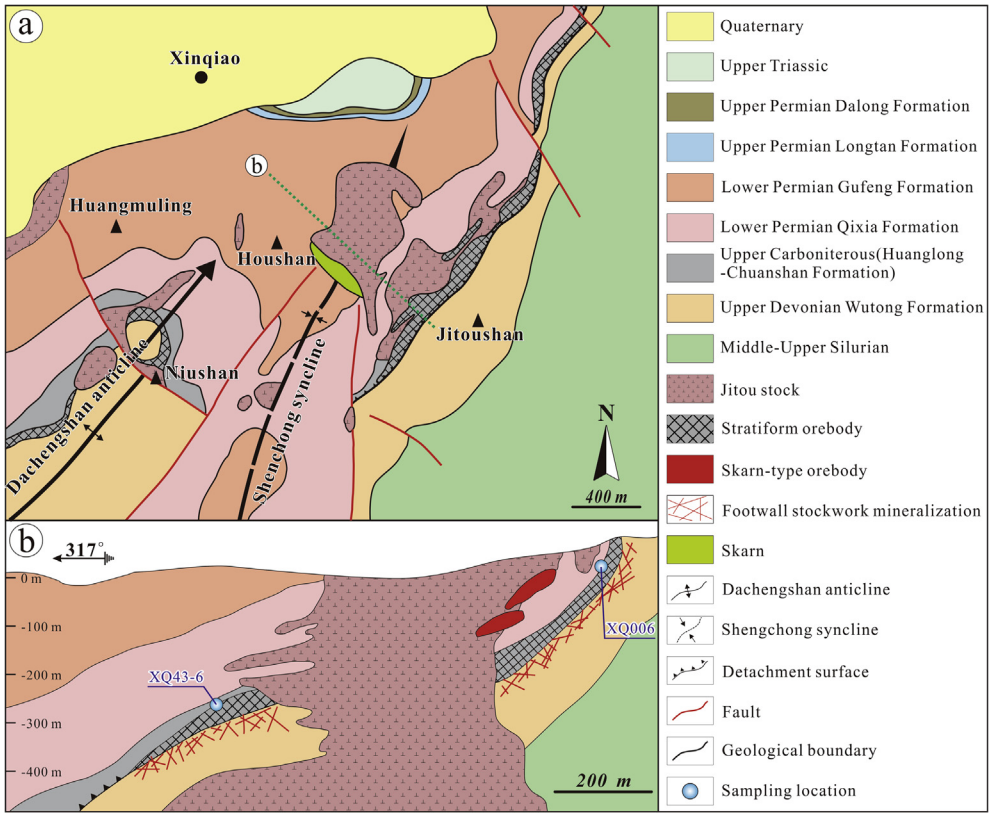

Fig. 3. (a) Geological map and (b) representative cross section of the Xinqiao Cu–S–Fe–Au deposit (after Tang et al., 1998 and Zang et al., 2004, respectively).

mineralization into five stages, namely early skarn (Stage I, dominated by garnet and diopside), late skarn (Stage II, featured by abundant epidote), metallic oxide (Stage III, dominated by hematite and magnetite), colloform pyrite (Stage IV, dominated by colloform pyrite) and quartz-sulfide (Stage V, featured by abundant quartz, chalcopyrite and pyrite).

3. Sampling and analytical methods

Two garnet skarn samples were collected from the top of the stratiform orebody in the southwest part of the 25 m platform at the Xinqiao open pit (XQ006; Fig. 4a) and in the stratiform orebody in the E16 stope at −270 m depth (XQ43-6; Fig. 4b). Garnet in sample XQ006 occurs as marble-intruding vein (garnet + diopside + epidote + quartz ≫ magnetite) (Fig. 4a). Sample XQ43-6 contains mainly garnet and diopside, and is crosscut by quartz ± pyrite veins (Fig. 4b).

Laser mount preparation and petrographic microscopy were conducted at the Key Laboratory of Metallogenic Prediction of Nonferrous Metals and Geological Environment Monitor (Central South University), Changsha, China.

EPMA analysis, mainly including in-situ major elements analysis, EPMA mapping and back-scattered electron (BSE) observation, was carried out in the School of Geosciences and Info-Physics of the Central South University, using a 1720 EPMA (Shimadzu Corporation, Japan). Analytical parameters include 15 kv (acc. voltage), 2.0×10^{-8} A (probe current) and 1 μm (spot size), and with 0.01% detection limit.

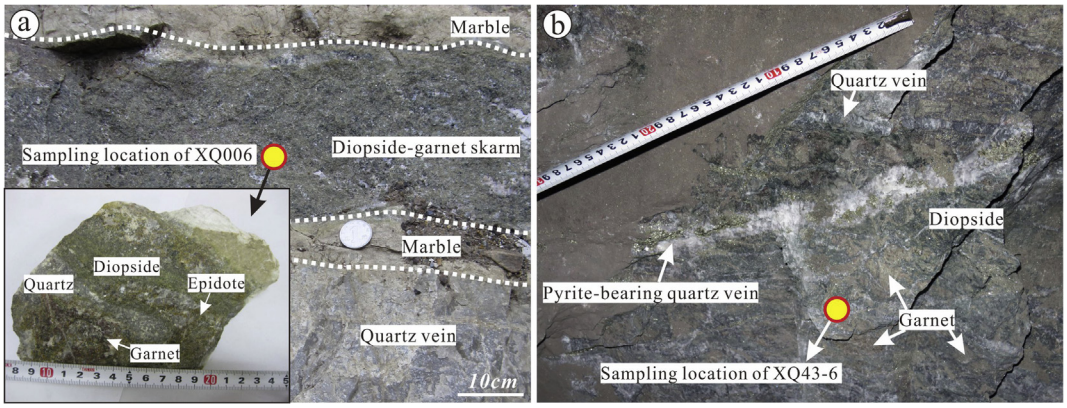

Fig. 4. (a) Garnet–diopside skarn outcrop and hand specimen for Sample XQ006. (b) Garnet–diopside skarn outcrop and hand specimen for Sample XQ43-6, showing the skarn crosscut by late quartz ± pyrite veins.

Subsequently, garnet LA-ICP-MS trace element analysis was carried out at the approximate points analyzed by EPMA at the Testing Center of the China Metallurgical Geology Bureau (Shandong office). The ablation was conducted using a pulsed 193 nm ArF Excimer (COMPexPRO CO2F Geolas) with a laser power of 8.5 J/cm^2 pulse energy at a repetition rate of 8 Hz, coupled to an Agilent 7500a quadrupole ICP-MS. Helium was used as a carrier gas to provide efficient aerosol transport to the ICP and to minimize aerosol deposition. The diameter of the laser ablation crater was 30 μm. The total ablation time was 110 s, comprising 30 s for the blank signal, 55 s for ablation, and 25 s for the residual signal. The zircon standard 91500 was used as an external standard and analyzed twice every five analyses. An external standard of NIST610 glass was analyzed once every 10 analyses to normalize U, Th, Pb, and other trace elements. The resultant data were processed using ICPMSDataCal (Liu et al., 2010). Elements analyzed include rare earth element (REE) and 13 trace elements (Y, Cs, Rb, Ba, Th, U, Nb, Ta, Pb, Sr, Zr, Hf and Ti).

4. Results

4.1. Garnet petrography

Under the microscope, the Xinqiao garnets are usually euhedral (Fig. 5a) or anhedral granular (Fig. 5b, c), contains no distinct oscillatory zoning and coexist with diopside. Locally, epidote occurs among garnet grains (Fig. 5a) or replaces (or corrodes) them (Fig. 5b, c).

Three different color gradients (dark gray, gray and light gray) were identified under BSE for the garnets (Fig. 5d–f). Dark gray garnet is anhedral granular and always occurs in the core of individual garnet grains (Fig. 5d–f). Gray garnet occurs either around dark gray garnet core (Fig. 5d–f), or forms clear oscillatory zoning with light gray garnet in the rim (Fig. 5d and f). Gray garnet is in conformable contact with light gray garnet, and thus their oscillatory zoning probably reflects garnet growth zoning.

EPMA mapping data of garnets not only provides mineral textural features, but also reveals the major element distribution (such as Al and Fe). The EPMA mapping shows that the dark gray and light gray garnets (under BSE imaging) have the highest Al and the lowest Fe, and the lowest Al and the highest Fe, respectively. The Al and Fe contents of gray garnet range between the dark gray and light gray garnets. Dark gray garnet cores were in some places replaced by gray garnet, leaving behind only some dark gray garnet residues (Figs. 5d–f and 6). This, and the different Al and Fe contents, indicates that the dark gray and gray garnets belong to two different generations. The gray garnet has more Al and less Fe than the light gray garnet, but they form clear oscillatory zonation pattern with conformable contact among them (Figs. 5d–f and 6), which reveal that the gray and light gray garnets probably belong to the same generation.

Therefore, we infer that there are two garnet generations at Xinqiao: the early garnet generation (Grt1) corresponds to the dark gray garnet core under BSE, and the late garnet generation (Grt2) comprises the gray garnet replacement of the dark gray core and the light gray ± gray garnet oscillatory zoning (Fig. 5d–f).

4.2. Major element geochemistry

A total of 29 EPMA spot analyses were completed on the two garnet samples, including two spots on Grt1, four spots on Grt2 core, five spots on Grt2 (gray) rims and 18 spots on Grt2 (light gray) rims. The results indicate that Grt1 has SiO_2, CaO and FeO concentrations of 36.31–36.39 wt.%, 34.28–34.91 wt.% and 17.19–17.79 wt.%, respectively. The SiO_2, CaO and FeO concentrations of Grt2 core vary from 34.15 wt.% to 36.08 wt.%, 33.51 wt.% to 34.27 wt.% and 24.16 wt.% to 26.89 wt.%, respectively. In terms of Grt2 rims, the gray rims have SiO_2, CaO and FeO concentrations of 34.97–35.64 wt.%, 32.87–33.72 wt.% and 26.04–28.47 wt.%, respectively, while the light gray rims vary from 32.93–35.68 wt.%, 32.34–33.47 wt.% and 30.05–32.33 wt.%, respectively (Table 1).

EPMA data show that the Xinqiao garnets were formed from grossular – andradite solid solution and range from pure andradite And_{100} to $And_{50}Gro_{46}$ with <4% uvarovite, pyrope and spessartine altogether (Fig. 7; Table 1). Grt1 contains nearly equal amount of andradite and grossular (i.e., grandite), the Grt2 cores and (gray) rims are dominated by andradite, and the Grt2 (light gray) rims contain almost pure andradite (Fig. 7).

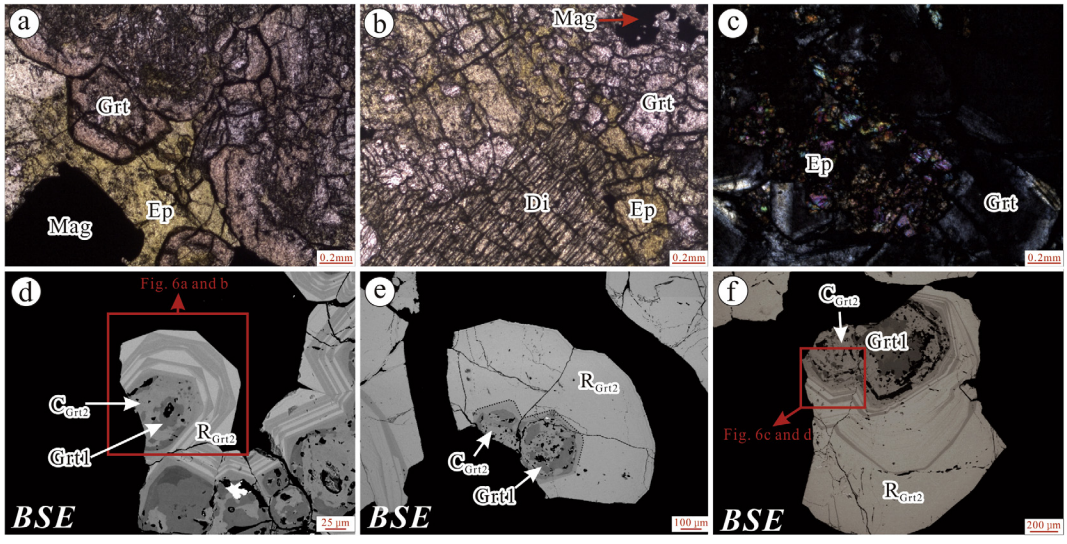

Fig. 5. Photomicrographs of the Xinqiao garnets. (a) Garnet and diopside replaced by epidote (PPL); (b) Epidote among garnets (PPL); (c) Epidote locally corrodes garnets (CPL); (d) and (f) Grt1 replaced by Grt2 in the garnet core, which is surrounded by oscillatory (gray and light gray) growth zoning (BSE image); (e) Grt1 replaced by Grt2 in the garnet core, which is surrounded by light gray rim (BSE image). Abbreviations: Grt = garnet, Ep = epidote, Di = diopside, Mag = magnetite, Grt1 = the early generation of garnets, Grt2 = the late generation of garnets, C_{Grt2} = the core of the late generation of garnets, R_{Grt2} = the rim of the late generation of garnets.

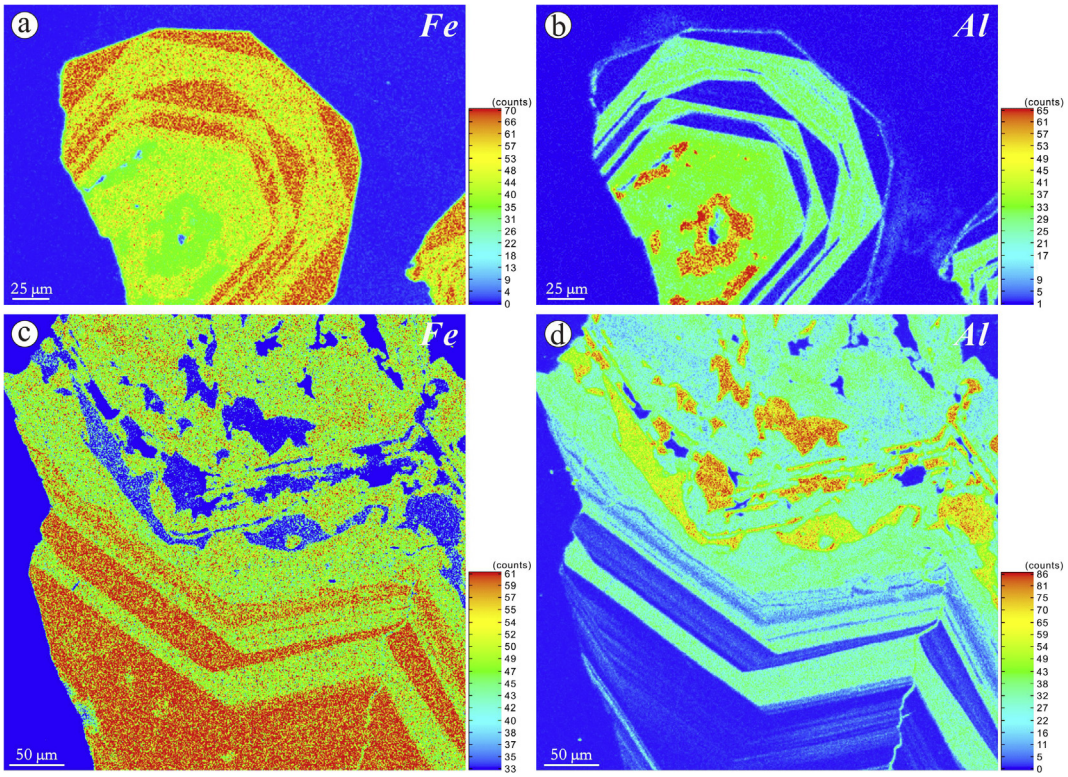

Fig. 6. EPMA element mapping of (a, c) Fe and (b, d) Al for the Xinqiao garnets.

4.3. Trace element geochemistry

A total of 19 LA-ICP-MS spot analyses were conducted on the two garnet samples, including nine spots on grandite (two on Grt1, four on Grt2 core and three on Grt2 rims) and ten spots on the Grt2 andradite rims. Rare earth element and trace element data of the Xinqiao garnets are shown in Tables 2 and 3, respectively.

In general, the grandite is HREE-enriched (ΣHREE = 13.19–38.06 ppm, average 22.35 ppm), and with low ΣLREE/ΣHREE (0.53–1.48, average 0.94), La_N/Yb_N (0.06–0.66, average 0.19) and negative Eu anomalies (0.50–0.84, average 0.67), whereas the andradite is HREE-depleted (ΣHREE = 0.65–3.34 ppm, average 1.71 ppm), with high ΣLREE/ΣHREE (6.31–40.07, average 19.43), La_N/Yb_N ratios (1.50–81.68, average 26.51) and positive Eu anomalies (1.30–4.14, average 2.56). Nevertheless, the grandite and andradite have similar ΣLREE. In addition, although all grandite contains similar REE patterns, ΣREE, ΣHREE and ΣLREE decrease from Grt1 through the Grt2 core to the Grt2 rim (Fig. 8; Table 2).

The Xinqiao garnets are generally depleted in large ion lithophile elements (LILEs), and contain lower Rb, Sr and Ba than average primitive mantle (Sun and McDonough, 1989). In contrast, their Cs, Th and U are higher than the average primitive mantle. Niobium, Ta, Hf, Y and Ti are enriched in the grandite but depleted in the andradite, compared to the average primitive mantle (Fig. 9; Table 3).

5. Discussion

5.1. Origin of Xinqiao garnets

Some previous attempts to identify the garnet origins by using REE patterns revealed that garnets of the same origin could have various REE patterns (Vander and Andre, 1991; Zhao et al., 1999; Zhao et al., 2007; Hong et al., 2012; Zheng et al., 2012). Gaspar et al. (2008) pointed out that the garnet REE patterns may be less dependent on its origin, but more dependent on the external factors (such as water/rock (W/R) ratios and metasomatic dynamics) and physicochemical conditions during formation. Therefore, the distinct REE patterns of Xinqiao garnet may not be able to provide direct indication for the origin.

As mentioned above, skarn minerals can be formed via four kinds of geological processes. There is no distinct regional metamorphism at Tongling, indicating that the Xinqiao garnets were not products of regional metamorphism. The Xinqiao garnets are formed from grossular-andradite solid solution and have low MnO (0.19–0.89%), obviously different from garnet from submarine sedimentary exhalation, which is commonly almandine and/or spessartine due to the abundance of Mn and Fe on the seafloor (Gemmell et al., 1992; Burton et al., 1999). Melt and fluid-melt inclusions are suggested to be a direct indicator for magmatic garnets (Ling and Cheng, 1998; Xiao and Liu, 2002; Zheng et al., 2012), yet they were not found in the garnets from the Xinqiao stratiform orebody (Zhang, 2015). Bau and Dulski (1996) considered that neither partial melting or fractional crystallization could lead to fractionation of Y from Ho, and hence magmatic garnets would have Y/Ho close to the chondrite value (i.e., 28, Anders and Grevesse, 1989), but hydrothermal system can readily fractionate Y from Ho. Grt1 and Grt2 have Y/Ho ratios of 39.0–40.7 (average 39.8) and 29.8–67.9 (average 43.8), respectively, which suggests that the Xinqiao garnets are likely to be hydrothermal replacement-type rather than magmatic. Furthermore, previous studies on the Xinqiao stratiform orebody, including the H–O isotope data obtained from the ore-bearing quartz revealing the magmatic hydrothermal characteristics of ore-forming fluid (Liu, 2002), the Rb–Sr isotope isochron age for the quartz fluid inclusions from the footwall stockwork mineralization (138.0 ± 2.3 Ma; Zhang et al., 2017), which are close to the

Table 1
EMPA geochemical data (wt.%) of the Xinqiao garnets. "–": Below the detection limit.

Type	R_{Grt2} (light gray)	R_{Grt2} (light gray)	R_{Grt2} (light gray)	R_{Grt2} (light gray)	R_{Grt2} (light gray)	R_{Grt2} (light gray)	Grt1	C_{Grt2}	R_{Grt2} (light gray)	R_{Grt2} (gray)	R_{Grt2} (light gray)	R_{Grt2}(gray)	Grt1	C_{Grt2}	C_{Grt2}
Sample	XQ006	XQ006	XQ006	XQ006	XQ006	XQ006	XQ006	XQ006	XQ006	XQ006	XQ006	XQ006	XQ43-6	XQ43-6	XQ43-6
Spot No.	1	2	3	4	5	6	7	8	9	10	11	12	13	14	15
SiO_2	33.94	32.93	33.39	34.34	34.44	34.24	36.39	36.08	35.68	35.64	35.15	35.64	36.31	35.36	34.15
TiO_2	–	–	–	–	0.03	–	0.85	0.80	0.03	0.15	0.03	0.01	0.94	1.24	0.83
Al_2O_3	–	–	–	0.03	0.13	0.21	8.41	4.15	0.07	3.69	0.17	3.03	9.17	3.13	2.94
Cr_2O_3	0.01	–	0.02	–	–	0.03	–	0.05	0.01	–	–	–	0.17	0.13	0.02
FeO	31.68	32.33	30.83	31.81	31.14	31.18	17.79	24.16	32.10	26.04	31.04	26.65	17.19	25.36	26.89
MnO	0.39	0.48	0.42	0.36	0.34	0.30	0.60	0.33	0.25	0.32	0.19	0.35	0.89	0.31	0.30
MgO	0.03	–	0.01	0.02	0.03	0.02	0.29	0.13	0.06	0.07	0.05	0.04	0.31	0.20	0.19
CaO	32.34	32.76	32.85	33.47	33.24	33.25	34.91	34.27	33.14	33.63	33.29	33.61	34.28	33.76	33.51
Total	98.39	98.49	97.52	100.02	99.35	99.21	99.24	99.96	101.34	99.53	99.91	99.33	99.26	99.48	98.83
Si	2.94	2.88	2.93	2.93	2.95	2.94	2.97	2.98	2.98	2.98	2.98	2.99	2.95	2.95	2.90
Ti	0	0	0	0	0	0	0.05	0.05	0	0.01	0	0	0.06	0.08	0.05
Al	0	0	0	0	0.01	0.02	0.81	0.40	0.01	0.36	0.02	0.30	0.88	0.31	0.29
Cr	0	0	0	0	0	0	0	0	0	0	0	0	0.01	0.01	0
Fe^{3+}	2.04	2.08	2.02	2.03	2.00	2.00	1.08	1.50	2.00	1.63	1.98	1.68	1.05	1.59	1.70
Fe^{2+}	0.02	0.02	0	0	0	0	0	0	0.02	0	0	0	0	0	0
Mn	0.03	0.04	0.03	0.03	0.02	0.02	0.04	0.02	0.02	0.02	0.01	0.02	0.06	0.02	0.02
Mg	0	0	0	0	0	0	0.04	0.02	0.01	0.01	0.01	0.01	0.04	0.02	0.02
Ca	3.00	3.07	3.09	3.06	3.05	3.06	3.05	3.04	2.97	3.01	3.03	3.02	2.98	3.02	3.05
Ura	0.06	0	0.09	0	0	0.11	0	0.21	0.02	0	0	0	0.60	0.52	0.07
And	99.94	100.00	99.91	99.83	99.18	98.62	53.97	75.35	99.55	78.34	98.93	81.94	49.91	80.61	82.56
Pyr	0	0	0	0.08	0.16	0.10	1.34	0.65	0.30	0.33	0.24	0.18	1.42	1.00	0.96
Spe	0	0	0	0.09	0.66	0.88	1.58	0.93	0.13	0.90	0.56	1.00	2.29	0.88	0.85
Gro	0	0	0	0	0	0.29	43.11	22.87	0	20.43	0.27	16.88	45.78	16.99	15.56
Alm	0	0	0	0	0	0	0	0	0	0	0	0	0	0	0

Type	R_{Grt2} (light gray)	R_{Grt2} (light gray)	R_{Grt2} (gray)	R_{Grt2} (light gray)	R_{Grt2} (gray)	R_{Grt2} (light gray)	C_{Grt2}	R_{Grt2} (light gray)	R_{Grt2} (light gray)	R_{Grt2} (light gray)	R_{Grt2} (gray)	R_{Grt2} (light gray)	R_{Grt2} (light gray)	R_{Grt2} (light gray)
Sample	XQ43-6	XQ43-6	XQ43-6	XQ43-6	XQ43-6	XQ43-6	XQ43-6	XQ43-6	XQ006	XQ006	XQ006	XQ006	XQ006	XQ006
Spot No.	16	17	18	19	20	21	22	23	24	25	26	27	28	29
SiO_2	34.48	33.30	35.00	34.53	35.15	34.52	34.43	34.51	34.56	34.35	34.97	34.63	35.23	34.96
TiO_2	0.01	0.07	0.57	0.02	0.18	–	0.82	–	0.06	–	0.10	–	0.03	0.03
Al_2O_3	0.09	0.69	3.08	0.37	2.31	0.12	2.73	0.19	0.03	–	1.95	0.08	0.56	0.07
Cr_2O_3	–	–	–	–	–	0.06	0.10	–	0.01	–	–	–	–	–
FeO	31.87	30.40	26.34	31.10	28.05	31.18	26.05	32.11	31.77	31.08	28.47	32.21	30.05	31.75
MnO	0.33	0.32	0.32	0.22	0.24	0.35	0.38	0.32	0.28	0.26	0.26	0.32	0.22	0.44
MgO	0.01	0.09	0.12	0.05	0.11	0.12	0.20	0.01	0.05	0.06	0.05	0.09	0.08	0.01
CaO	33.19	32.44	32.87	33.32	33.49	33.34	33.63	33.19	33.01	33.24	33.72	33.21	32.94	32.85
Total	99.97	97.31	98.29	99.62	99.52	99.68	98.32	100.32	99.76	98.99	99.53	100.53	99.10	100.09
Si	2.94	2.91	2.96	2.95	2.96	2.95	2.93	2.93	2.95	2.96	2.96	2.94	3.00	2.97
Ti	0	0	0.04	0	0.01	0	0.05	0	0	0	0.01	0	0	0
Al	0.01	0.07	0.31	0.04	0.23	0.01	0.27	0.02	0	0	0.19	0.01	0.06	0.01
Cr	0	0	0	0	0	0	0.01	0	0	0	0	0	0	0
Fe^{3+}	2.03	1.98	1.68	1.99	1.77	1.99	1.66	2.03	2.03	2.00	1.80	2.03	1.92	2.01
Fe^{2+}	0	0	0	0	0	0	0	0.02	0	0	0	0.01	0	0.01
Mn	0.02	0.02	0.02	0.02	0.02	0.03	0.03	0.02	0.02	0.02	0.02	0.02	0.02	0.03
Mg	0	0.01	0.02	0.01	0.01	0.02	0.03	0	0.01	0.01	0.01	0.01	0.01	0
Ca	3.03	3.04	2.98	3.05	3.02	3.05	3.07	3.02	3.02	3.06	3.06	3.02	3.00	2.99
Ura	0	0	0	0.01	0	0.24	0.40	0	0.02	0	0	0	0	0
And	99.45	95.74	81.37	97.70	86.17	99.05	83.20	98.86	99.77	100.00	88.28	99.51	96.51	99.60
Pyr	0.06	0.49	0.59	0.28	0.56	0.62	0.99	0.06	0.20	0	0.27	0.48	0.43	0.03
Spe	0.48	0.96	0.93	0.64	0.68	0.09	1.09	0.94	0	0	0.75	0.01	0.67	0.37
Gro	0	2.81	17.11	1.37	12.60	0	14.33	0.14	0	0	10.70	0	2.39	0
Alm	0	0	0	0	0	0	0	0	0	0	0	0	0	0

Note: All the calculations are based on 12 oxygens. Abbreviations: Ura – uvarovite; And – andradite; Pyr – pyrope; Spe – spessartine; Gro – grossular; Alm – almandine.

SHRIMP zircon U–Pb age (140.4 ± 2.2 Ma; Wang et al., 2004) of Jitou quartz diorite stock in Xinqiao mining area, and iron isotope compositions of pyrites (δ^{57}Fe ranges from −1.22‰ to 0.15‰; Wang et al., 2011, 2013) similar to the pyrites in skarn system (δ^{57}Fe ranges from −2.58‰ to 1.62‰; Graham et al., 2004), indicate that the stratiform orebody may have been associated with the magmatic-hydrothermal fluids derived from Jitou stock. Additionally, the geochemical feature that early garnets tend to be Al-enriched and later ones Fe-enriched, is consistent with most garnets related to skarn Cu and Fe deposits worldwide (Fig. 7; Einaudi et al., 1981; Nakano et al., 1989; Meinert, 1992, 1997). Therefore, the garnets in the stratiform orebody are likely to be a magmatic-hydrothermal replacement origin, associated with the Jitou stock.

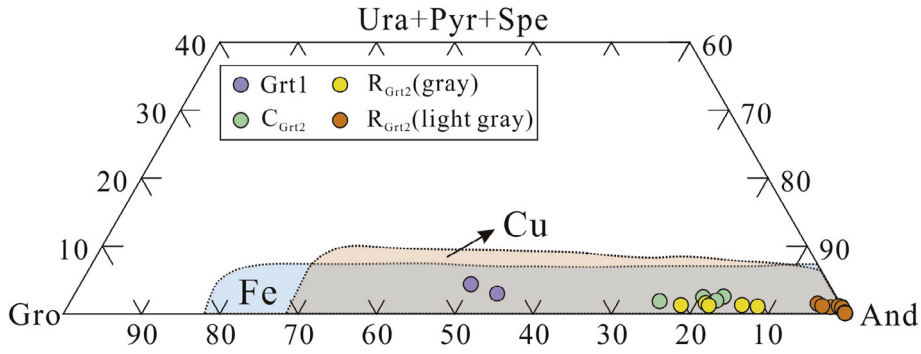

Fig. 7. Classification diagram for the Xinqiao garnets. The Fe and Cu skarn deposit fields are from Meinert (1992). Abbreviations: Gro = grossular; And = andradite; Ura = uvarovite; Pyr = pyrope; Spe = spessartine; C_{Grt2} = Grt2 core, R_{Grt2} (gray) = Grt2 (gray) rim; R_{Grt2} (light gray) = Grt2 (light gray) rim.

Based on the REE data, the HREE-enriched grandite may have formed by direct crystallization from HREE-rich fluids, whereas the HREE-depleted andradite Grt2 rims may have originated from HREE-depleted fluids. Al-bearing garnets are able to fractionate HREE from LREE (Scherer et al., 2000; Pertermann et al., 2004; Gaspar et al., 2008). Formation of Grt1 grandite may have depleted the HREEs in the hydrothermal fluids, consequently forming the LREE-rich Grt2 andradite rims.

5.2. Physicochemical evolution of hydrothermal fluids

5.2.1. pH

In terms of factors that control water-rock interaction, Bau (1991) demonstrated that pH significantly affects REE fractionation of skarn hydrothermal fluids. Under nearly neutral pH, the REE patterns of the fluids are relatively HREE-enriched and LREE-depleted with negative or no Eu anomaly (Bau, 1991), which are consistent with the Xinqiao grandite REE patterns (Fig. 8), suggesting that the grandite may have formed under nearly neutral pH (Gaspar et al., 2008; Zhai et al., 2014).

The presence of magnetite and pyrrhotite in the Xinqiao stratiform orebody, indicates less oxidized environment with fO_2 below the hematite-magnetite buffer (Gaspar, 2005), in which Eu was likely to occur as Eu^{2+} (Gaspar et al., 2008). Without taking the oxygen fugacity into account, the Eu^{3+}/Eu^{2+} redox potential in hydrothermal fluids depends primarily on temperature and speciation and less on pH or pressure (Sverjensky, 1984; Bau, 1991). Speciation can extend the Eu^{3+} stability in hydrothermal fluids at low temperatures, whereas Eu^{2+} ions dominate at above 250 °C (Sverjensky, 1984). Fluid inclusions in the Xinqiao garnets (from the stratiform orebody) homogenized at >324 °C (Zhang, 2015). Therefore, Eu^{2+} ions were likely to dominate, which favors Eu^{2+} substituting Ca^{2+} readily in garnet crystals in the form of isomorphism based their same valence and similar ionic radius. Especially, under mildly acidic conditions, the REE patterns are significantly controlled by the presence of Cl^- (Bau, 1991), which can enhance the stability of soluble Eu^{2+} except for REE^{3+} and form distinct positive Eu anomalies (Gaspar et al., 2008; Mayanovic et al., 2002, 2007; Allen and Seyfried, 2005). The Cl^- concentration in fluid inclusions trapped in Xinqiao garnet reaches up to 3.296 μg/g (Zhang, 2015), which could facilitate the transport of Eu^{2+} in hydrothermal fluids. Since the andradite has distinct positive Eu anomalies, we inferred that the Xinqiao andradite may have formed under mildly acidic condition, consistent with the Crown Jewel gold deposit, North America (Gaspar et al., 2008) and the Xieertala Fe–Zn skarn deposit, northern China (Zhai et al., 2014).

5.2.2. Oxygen fugacity

As mentioned above, Eu^{2+} ions were likely to dominate in hydrothermal fluids, indication of the low Eu^{3+}/Eu^{2+} redox potential, and the hydrothermal fluids were under less oxidized cindition with fO_2 below the hematite-magnetite buffer in general. Additionally, the incorporation of U into grandite or andradite is only possible by coupled substituting Ca^{2+} in the dodecahedral position, on the basis of similar ionic radius and charge balance (Shannon, 1976; Smith et al., 2004; Gaspar et al., 2008; Dziggel et al., 2009). U^{4+} is more likely to substitute into garnet than U^{6+} (Smith et al., 2004). Thus, the U concentrations in different parts of the garnet crystals can indicate the relative oxygen fugacity (fO_2) of hydrothermal fluids during the garnet formation. Decreasing fO_2 of the fluid system could reduce U solubility and in turn increase U incorporation into garnet. Grt1, and the Grt2 grandite cores and rims have similar U concentrations of 6.230–7.143 ppm (average 6.686 ppm), 4.590–4.193 ppm (average 4.885 ppm) and 1.122–5.675 ppm (average 3.795 ppm), respectively, while the Grt2 andradite rims have much higher U concentrations (2.217–19.416 ppm, average 10.769 ppm). Thus, fO_2 during the grandite formation was likely to be higher than that of andradite.

5.3. Metasomatic dynamics of Xinaqiao garnets

As discussed above, the Xinqiao garnets from the stratiform orebody were likely originated from magmatic-hydrothermal replacement. Magmatic-hydrothermal skarns could be formed by diffusive metasomatism or infiltration metasomatism (Bau, 1991; Gaspar et al., 2008). Diffusive metasomatism would produce fluids and alteration products in which REE composition is buffered by the host rock composition due to long pore fluid residence under closed system conditions (e.g., the intrusive contact between igneous rock and carbonate), and these fluids have nearly neutral pH with hydroxide and carbonate as the main complexing agents. Infiltration metasomatism, associated with an increase in W/R ratio, would produce fluids and mineral assemblages buffered by mildly acidic external derived fluids with chloride complexes that can be important in Eu^{2+} transport, under open system conditions (e.g., rock fractures) (Gaspar et al., 2008).

The absence of oscillatory zoning in Grt1 and the Grt2 cores indicates that they were formed under a relatively stable and closed system condition. Additionally, the magmatic-hydrothermal fluids during the formation of Grt1 and the Grt2 cores may have had a nearly neutral pH, and thus these earlier garnets may have formed via diffusive metasomatism by fluids equilibrated with the host rocks. In comparison, Grt2 rims have clear oscillatory zones and were likely formed under an oscillatory physicochemical and open system condition, consistent with the unconformity between the Upper Devonian Wutong Formation quartz sandstone and the Upper Carboniferous Huanglong Formation limestone. Moreover, the hydrothermal fluids during the formation of Grt2 andradite rims may have had a mildly acidic pH,

Table 2
LA-ICP-MS rare earth elements data (ppm) of the Xinqiao garnets.

Type	Grt1		C_{Grt2}				R_{Grt2} (gray zones)			R_{Grt2} (light gray zones)								
Sample	XQ006	XQ43-6	XQ006	XQ43-6	XQ43-6	XQ43-6	XQ006	XQ006	XQ43-6	XQ006	XQ43-6	XQ43-6	XQ43-6	XQ43-6	XQ006	XQ006	XQ006	XQ006
Spot No.	7	13	8	14	15	22	10	12	18	11	16	17	19	21	23	24	25	27	29
La	1.783	1.795	0.448	0.583	0.464	0.459	1.702	0.220	0.936	3.709	3.725	13.962	8.114	7.912	5.251	3.896	3.523	7.632	1.259
Ce	12.910	12.206	3.419	2.424	2.448	2.369	7.306	1.794	3.440	18.457	5.517	14.277	9.264	13.868	3.510	18.108	17.356	15.105	7.919
Pr	3.709	4.146	1.389	0.901	0.875	0.793	1.179	0.810	0.688	3.352	0.689	1.861	1.376	1.640	0.433	3.011	2.950	1.716	1.956
Nd	19.648	29.032	11.438	6.240	6.473	6.228	5.399	5.641	3.713	12.106	1.979	3.792	3.551	3.758	1.442	9.323	9.434	3.525	8.392
Sm	4.323	7.292	3.132	2.268	2.342	2.760	1.913	1.781	1.496	1.142	0.258	0.411	0.556	0.367	0.215	1.048	1.242	0.236	1.057
Eu	1.198	1.970	0.864	0.529	0.551	0.521	0.714	0.546	0.467	1.376	0.159	0.308	0.266	0.129	0.098	1.258	1.278	0.206	0.484
Gd	6.883	9.342	4.403	3.988	3.745	3.625	3.456	2.650	2.649	0.818	0.155	0.467	0.612	0.093	0.243	0.763	0.743	0.113	0.785
Tb	1.104	1.567	0.760	0.777	0.732	0.730	0.460	0.471	0.509	0.069	0.025	0.035	0.061	0.054	0.049	0.086	0.134	0.051	0.148
Dy	7.994	10.156	5.825	6.352	5.568	6.033	3.425	3.654	3.969	0.459	0.241	0.303	0.322	0.255	0.256	0.632	0.846	0.284	0.813
Ho	1.880	2.343	1.409	1.527	1.413	1.525	0.794	0.883	1.111	0.089	0.028	0.041	0.077	0.034	0.102	0.124	0.182	0.047	0.232
Er	5.147	6.358	3.995	4.984	4.461	4.975	2.676	2.413	3.066	0.385	0.111	0.176	0.182	0.079	0.238	0.355	0.511	0.209	0.595
Tm	0.660	1.082	0.636	0.763	0.667	0.697	0.371	0.334	0.448	0.037	0.012	0.016	0.031	0.016	0.053	0.029	0.085	0.028	0.091
Yb	5.330	6.229	4.323	5.322	4.593	4.909	1.858	2.444	2.962	0.238	0.065	0.123	0.202	0.138	0.199	0.350	0.420	0.202	0.602
Lu	0.758	0.985	0.693	0.764	0.711	0.759	0.281	0.343	0.476	0.052	0.011	0.025	0.046	0.021	0.041	0.045	0.101	0.031	0.075
ΣREE	73.328	94.504	42.735	37.422	35.042	36.385	31.533	23.985	25.929	42.289	12.975	35.796	24.659	28.365	12.130	39.029	38.806	29.385	24.407
ΣLREE	43.571	56.441	20.690	12.946	13.153	13.130	18.214	10.792	10.739	40.142	12.327	34.610	23.126	27.674	10.949	36.644	35.783	28.420	21.067
ΣHREE	29.757	38.063	22.044	24.477	21.889	23.255	13.320	13.193	15.190	2.146	0.648	1.185	1.533	0.691	1.181	2.385	3.022	0.965	3.340
LREE/HREE	1.464	1.483	0.939	0.529	0.601	0.565	1.367	0.818	0.707	18.702	19.019	29.203	15.085	40.072	9.269	15.367	11.840	29.435	6.308
La_N/Yb_N	0.240	0.207	0.074	0.079	0.072	0.067	0.657	0.065	0.227	11.158	40.931	81.680	28.850	41.011	18.922	7.974	6.023	27.059	1.500
δEu	0.669	0.730	0.711	0.533	0.567	0.504	0.840	0.768	0.710	4.145	2.246	2.140	1.386	1.558	1.312	4.107	3.754	3.401	1.557
δCe	0.906	0.779	0.677	0.663	0.717	0.753	1.219	0.620	1.005	1.184	0.785	0.594	0.621	0.895	0.429	1.229	1.235	0.982	0.999

Note: REE normalized to chondrite (Sun and McDonough, 1989).

and the REE patterns of Grt2 andradite rims are similar to those of the common magmatic-hydrothermal fluids, which have in general very low REE contents (LREE-enriched and HREE-depleted) and positive Eu anomalies (Flynn and Burnham, 1978; Ayers and Eggler, 1995; Kravchuk et al., 1995; Reed et al., 2000), indicative of external derived magmatic-hydrothermal fluids. Therefore, Grt2 rim may have formed primarily via infiltration metasomatism. Here we propose a possible formation process for the Xinqiao garnets.

At Xinqiao, diffusive metasomatism may have mainly occurred along the intrusive contact zone between the Upper Carboniferous Huanglong Formation limestone and quartz diorite of the Jitou stock. When magmatic-hydrothermal fluids entered the intrusive contact zone, Ca in the Huanglong Formation limestone, and Si and Al in the Jitou quartz diorite may have been remobilized and interact to form Grt1 grandite. Subsequently, the ore-forming fluids (with some remobilized Al unused in the previous Grt1 formation) may have percolated into the low-pressure unconformity between the Wutong and Huanglong formations, and interacted with the limestone to form the Grt2 grandite cores via diffusive metasomatism. Additionally, this migration of the ore-forming fluids from the intrusive contact to the unconformity would probably cause that a few Grt1 particles forming near the intersection between Jitou stock and the unconformity had been 'poured' into the unconformity and replaced by the later Grt2 cores. Iron isotopes (δ^{57}Fe ranges from −1.22‰ to 0.15‰) reveal that Fe in the Xinqiao deposit may have been derived from magma related to Jitou stock (Wang et al., 2011, 2013), which suggests that the magmatic-hydrothermal fluids for ore-forming is enriched in Fe. Therefore, with ore-forming fluids probably continuously entering the unconformity, the main component of fluids maybe gradually changed from enriched Si and Al buffered by the host rock (limestone and quartz diorite) composition in the intrusive contact zone to enriched Fe derived by magmatic-hydrothermal fluids in the unconformity, with metasomatic dynamics for garnet growth changing from diffusive to infiltration metasomatism. Such change may have led to the Grt2 andradite rim formation.

5.4. Metallogenic implications

The Xinqiao stratiform orebody with the footwall stockwork mineralization mimics the dual structure of typical sedimentary exhalative (SEDEX) deposits (Sangster, 1990), and the colloform pyrite in the stratiform orebody displays typical synsedimentary texture. These two features were interpreted to be key factors of the Late Paleozoic submarine exhalative processes (Gu and Xu, 1986; Gu et al., 2000; Xu and Zhou, 2001; Xu et al., 2004). Previous studies have documented that the feeder zones of SEDEX deposits are typically rooted in a synsedimentary fault (Large, 1983; Goodfellow et al., 1993) and consist of brecciated and altered sedimentary rocks overprinted by veins and vein networks composed principally of quartz, Fe-Mn carbonates, and sulfides (Leach et al., 2005). However, the Tongling district was one part of the stable craton in the Carboniferous period, and there was no synsedimentary faults occurring in it (Huang, 1999). Furthermore, the breccia and Fe-Mn carbonates have not been found in the footwall of stratiform orebody and the footwall quartz-pyrite stockwork, respectively (Zhang et al., 2017), which contrasts to the typical SEDEX deposits. It seemingly provides further evidence for the Xinqiao SEDEX hypothesis that pyrite from the footwall stockwork mineralization were dated to be the Late Carboniferous (Re–Os; 319 ± 13 Ma; Guo et al., 2011), however, the initial $^{187}Os/^{188}Os$ (0.017) is much lower than those of typical SEDEX deposits, which range between average oceanic crust (~1) and seawater (~8) (Ravizza et al., 1996). Furthermore, the pyrite ^{187}Os vs. ^{187}Re ratios are confined in a fairly narrow range, which cannot most likely

Table 3
LA-ICP-MS trace elements data (ppm) of the Xinqiao garnets.

Type	Sample	Spot No.	Y	Hf	Ta	Th	U	Sc	Ti	Rb	Sr	Nb	Cs	Ba
Grt1	XQ006	7	76.448	4.591	0.341	0.291	6.230	12.586	4021.725	0.026	1.030	3.000	0.042	0.201
	XQ43-6	13	91.460	11.436	0.326	0.399	7.143	22.608	4315.785	1.198	13.545	2.581	0.729	4.012
C_{Grt2}	XQ006	8	57.332	8.144	0.474	0.664	5.054	18.438	4233.375	1.227	1.753	1.740	0.340	0.740
	XQ43-6	14	66.158	15.633	0.668	1.498	4.590	27.922	6001.759	0.380	1.845	2.059	0.081	0.857
	XQ43-6	15	57.547	11.618	0.551	1.197	4.702	20.609	4903.679	0.300	5.621	1.850	–	0.342
	XQ43-6	22	63.689	11.763	0.744	1.592	5.193	32.464	5776.972	1.310	1.231	2.626	0.267	1.204
R_{Grt2} (gray zone)	XQ006	10	31.157	2.237	0.135	0.617	5.675	4.143	1455.787	0.133	0.057	0.931	0.078	0.190
	XQ006	12	34.249	1.272	0.053	0.374	1.122	0.486	875.570	–	0.231	0.904	–	–
	XQ43-6	18	39.812	2.201	0.164	0.342	4.588	2.536	1583.877	–	0.072	0.736	–	0.102
R_{Grt2} (light gray zone)	XQ006	11	4.718	0.155	0.014	5.910	13.525	0.777	157.461	–	0.421	0.175	0.088	0.040
	XQ43-6	16	1.467	–	–	0.591	9.615	0.705	9.625	0.023	0.167	0.014	–	0.020
	XQ43-6	17	2.132	0.037	0.001	1.652	16.667	0.574	15.902	0.437	0.299	0.012	0.125	0.170
	XQ43-6	19	3.104	–	0.002	2.195	19.416	1.147	23.040	–	0.174	–	–	0.019
	XQ43-6	21	2.307	–	–	0.298	7.646	0.393	69.077	0.256	0.188	0.017	–	–
	XQ43-6	23	3.037	0.015	0.006	0.009	2.217	0.375	8.578	0.267	0.140	–	0.031	0.021
	XQ006	24	4.977	0.037	0.016	9.907	12.972	0.725	202.940	0.118	–	0.271	–	0.012
	XQ006	25	7.364	0.236	0.017	11.315	12.184	0.545	313.673	–	–	0.308	–	0.085
	XQ006	27	2.282	–	–	5.836	9.298	0.618	132.436	–	0.021	–	–	0.107
	XQ006	29	9.033	0.147	0.014	1.418	4.149	0.672	347.914	–	0.022	0.221	–	0.064

"–": Below the detection limit.

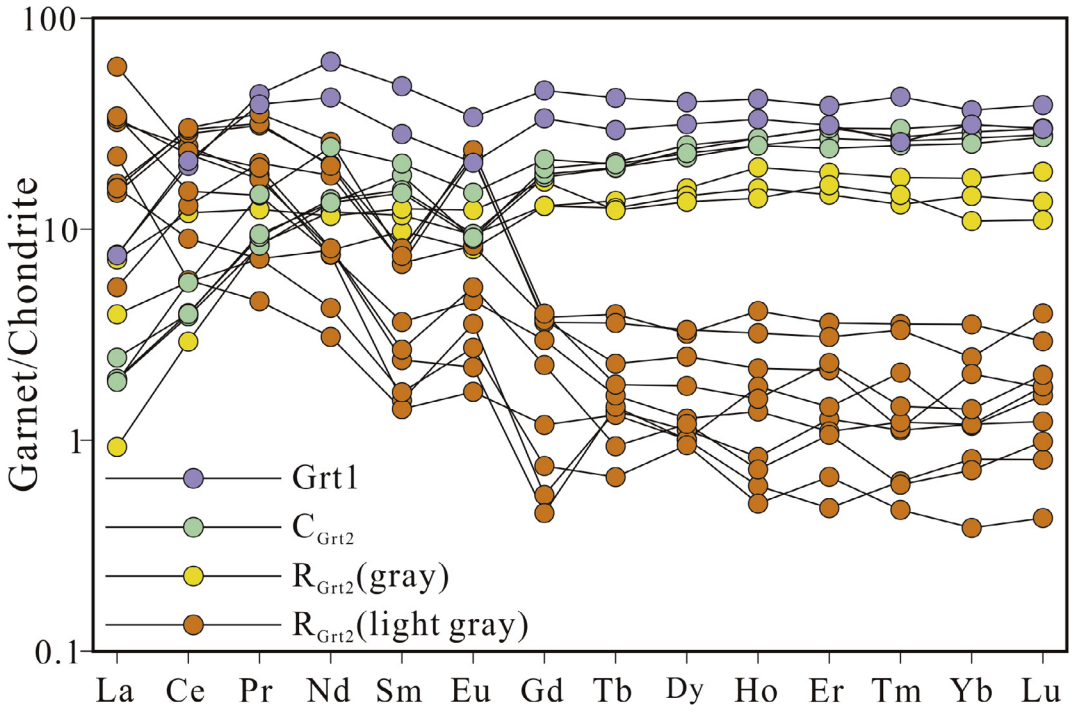

Fig. 8. Chondrite-normalized REE patterns of the Xinqiao garnets. Normalization values are from Sun and McDonough (1989).

reflect the true age of the footwall stockwork mineralization (Huang, 2011). As mentioned above, the Rb–Sr isochron age of fluid inclusions trapped in quartz from the footwall stockwork mineralization is close to zircon U–Pb dating of Jitou stock, and the initial $^{87}Sr/^{86}Sr$ value (0.71138 ± 0.00014) of the footwall stockwork mineralization is similar to that of the Jitou stock, but different from the value of the ore-hosting limestone (Zhang et al., 2017). These indicate that the Xinqiao footwall stockwork mineralization was likely to be genetically linked to the magmatic-hydrothermal fluids associated with the Jitou stock, but different from typical feeder zones of SEDEX deposits. Additionally, abundant pyrite occurs as colloform, fine grain and coarse grain in the Xinqiao stratiform orebody (Zhang et al., 2016), seemingly conforming to the highly variable grain sizes of sulfides in SEDEX deposits (Leach et al., 2005). However, the Fe isotope compositions ($\delta^{57}Fe$: −1.22‰ to 0.15‰; Wang et al., 2011), S isotope compositions ($\delta^{34}S_{CDT}$: −0.6‰ to 2.7‰; Zhang et al., 2016) and Co/Ni values (0.67–2.94, average 1.66; Zhang et al., 2016) of the Xinqiao colloform pyrite reveal its magmatic hydrothermal origin, rather than synsedimentary origin corresponding to the Xinqiao SEDEX hypothesis.

Garnet alteration could promote wallrock fracturing and thus migration of ore-forming fluids, water-rock interaction and ore-mineral deposition. Therefore, garnet alteration is regarded to be a preparatory stage for skarn mineralization (Karimzadeh, 2010; Ying et al., 2012). The Xinqiao garnets plot in the Cu and Fe skarn mineralization fields (Fig. 7), which indicates that the Xinqiao hydrothermal fluids had a Cu–Fe skarn mineralization potential (Meinert, 1992), consistent with the occurrence of chalcopyrite

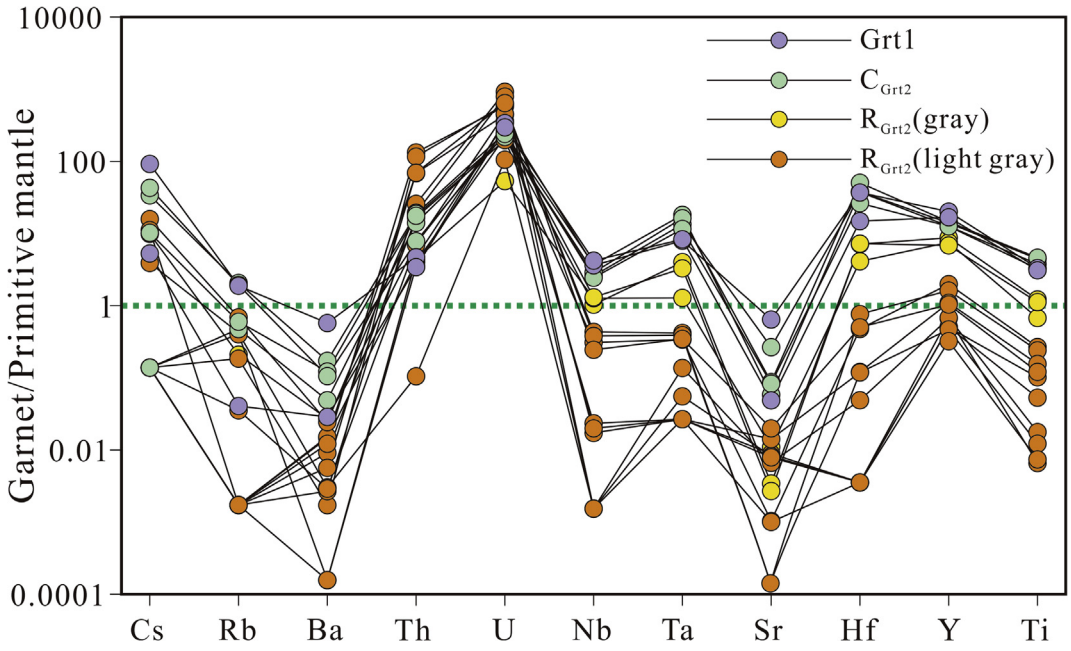

Fig. 9. Primitive mantle-normalized multi-element diagram of the Xinqiao garnets. Normalization values are from Sun and McDonough (1989).

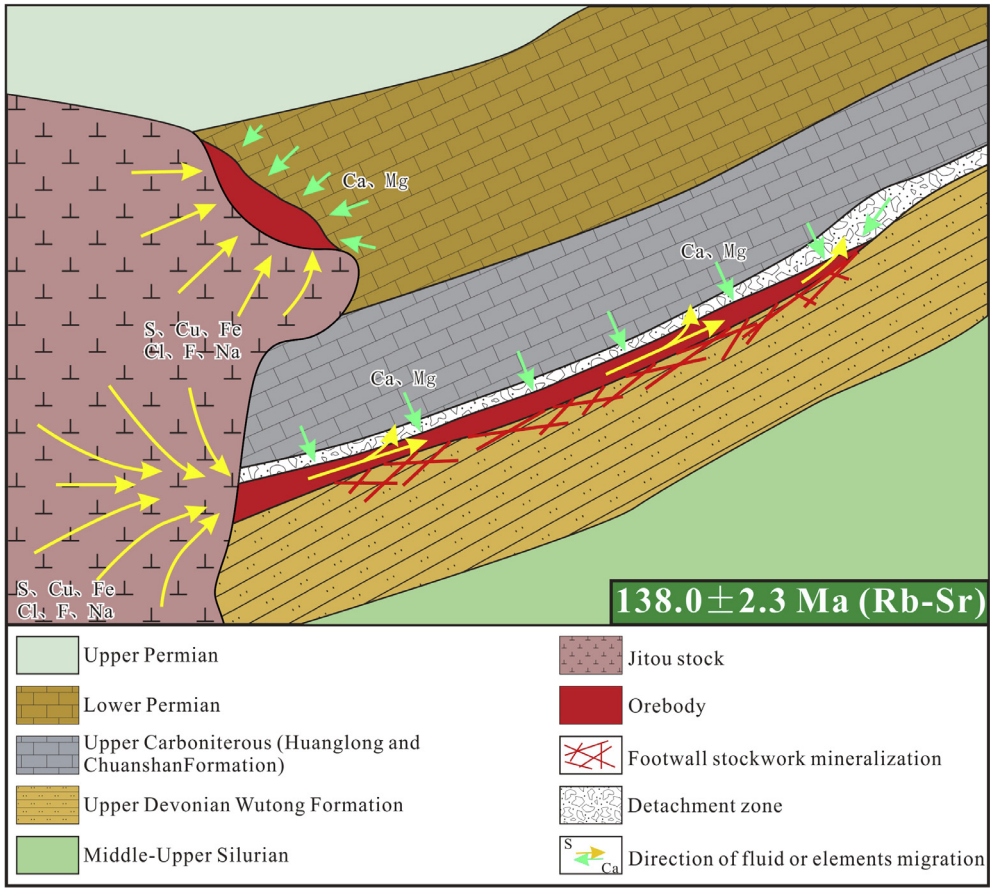

Fig. 10. Ore genesis model for the Xinqiao Cu–S–Fe–Au deposit (Zhang et al., 2017).

and magnetite as the main ore minerals at Xinqiao. Petrographic observation reveals that volumetrically the Grt2 andradite rims dominate the Xinqiao garnets (Fig. 5e and f), and therefore garnets from the Xinqiao stratiform orebody were likely formed primarily by infiltration metasomatism. The ore-hosting unconformity between the Upper Devonian Wutong Formation quartz sandstone

and the Upper Carboniferous Huanglong Formation limestone may have provided enough open space for the metasomatism. Magmatic-hydrothermal fluids derived from the Jitou stock may have preferentially infiltrated into the relatively low-pressure unconformity and interacted with Huanglong Formation limestone.

A magmatic-hydrothermal origin for the Xinqiao mineralization has been proposed in the past decades (Chang and Liu, 1983; Chang et al., 1991; Zhai et al., 1992; Meng, 1994, 1996; Pan and Done, 1999; Mao et al., 2009, 2011). Here we propose a modified tectono-metallogenic model for the Xinqiao mineralization.

From ca. 180 to 90 Ma, the eastern China continental margin may have evolved from an active continental margin to an intraplate setting, and the stress field may have changed from compressive to extensional (Qi et al., 2000). When the paleo-Pacific plate subduction began and the Yangtze continental crust delaminated, the structural orientation of the Middle-Lower Yangtze River Valley metallogenic belt may have changed from E- to NE-trending, and then to NNE-trending, and the resultant complex crustal-mantle interactions may have generated extensive magmatism (Mao et al., 2013; Wu et al., 2003). Under such a tectono-magmatic regime, the region between the Jitou–Shatanjiao basement fault and the NNE-trending fault zone was extended, leading to asthenospheric upwelling and associated magmatism (Zhang, 2015). The magmas may have migrated along the NE-trending Dachengshan anticline and the NNE-trending Shenchong syncline to form the NW-trending Jitou stock (Liu et al., 1996). Subsequently, magmatic-hydrothermal fluids enriched in ore-forming elements may have ascended and entered the intrusive contact and then the unconformity at Xinqiao in the Early Cretaceous (ca. 138.0 ± 2.3 Ma, Rb–Sr age for the fluid inclusions in quartz from the footwall stockwork mineralization; Zhang et al., 2017), which may have resulted in the formation of Grt1 and the Grt2 core by diffusive metasomatism and the Grt2 rims by infiltration metasomatism. After that, the further evolution of physicochemical conditions decreased the Cu solubility, precipitated pyrite and Cu sulfides and formed the Xinqiao mineralization (Fig. 10; Zhang et al., 2017).

6. Conclusions

(1) Garnets from the Xinqiao stratiform orebody can be divided into an early garnet (Grt1) and a late garnet (Grt2) generation. Grt1 and the Grt2 cores are grandite, while the Grt2 rims are andradite ± grandite.
(2) The grandite is rich in HREEs, and has low U, ΣLREE/ΣHREE, La_N/Yb_N and negative Eu anomalies, whereas the andradite is depleted in HREEs, and has high U, ΣLREE/ΣHREE, La_N/Yb_N and positive Eu anomalies.
(3) Garnets from the Xinqiao stratiform orebody may have resulted from magmatic-hydrothermal replacement.
(4) Hydrothermal fluids for Grt1 and the Grt2 cores may have been nearly neutral pH, oxidized and HREE-enriched, whereas those for the Grt2 rims may have experienced episodic inflections between a mildly acidic, reduced and HREE-depleted fluid and a near neutral, oxidized and HREE-enriched fluid.
(5) Grt1 and the Grt2 cores may have formed by diffusive metasomatism, whereas the Grt2 rims may have formed by infiltration metasomatism.
(6) The Xinqiao stratiform orebody may have formed from Early Cretaceous magmatic-hydrothermal fluids associated with the Jitou stock, similar to the skarn orebodies in the district.

Acknowledgements

This research was jointly funded by the CAS-SAFEA International Partnership Program for Creative Research Teams (20140491534), the Project of Innovation-driven Plan of the Central South University (2015CX008) and the Special Research Funding for the Public Benefit of the MLR China (200911007-4). We especially thank Feng-chun Li for helping with the LA-ICP-MS trace element analyses, and Dr Yu-zhou Feng for assisting with the EPMA analyses.

References

Allen, D.E., Seyfried, W.E., 2005. REE controls in ultramafic hosted MOR hydrothermal systems: an experimental study at elevated temperature and pressure. Geochim. Cosmochim. Acta 69, 675–683.
Anders, M., Grevesse, N., 1989. Abundances of the elements: meteoritic and solar. Geochim. Cosmochim. Acta 53, 197–214.
Ayers, J.C., Eggler, D.H., 1995. Partitioning of elements between silicate melt and H_2O-NaCl fluids at 1.5 and 2.0 GPa pressure: implications for mantle metasomatism. Geochim. Cosmochim. Acta 59, 4237–4246.
Bau, M., 1991. Rare-earth element mobility during hydrothermal and metamorphic fluid-rock interaction and the significance of the oxidation state of europium. Chem. Geol. 93, 219–230.
Bau, M., Dulski, P., 1996. Anthropogenic origin of positive gadolinium anomalies in river waters. Earth Planet. Sci. Lett. 143, 245–255.
Burton, K.W., Bourdon, B., Birck, J.L., Allègre, C.J., Hein, J.R., 1999. Osmium isotope variations in the oceans recorded by Fe-Mn crusts. Earth Planet. Sci. Lett. 171 (1), 185–197.
Cao, Y., Zheng, Z.J., Du, Y.L., Gao, F.P., Qin, X.L., Yang, H.M., Lu, Y.H., Du, Y.S., 2017. Ore geology and fluid inclusions of the Hucunnan deposit, Tongling, Eastern China: implications for the separation of copper and molybdenum in skarn deposits. Ore Geol. Rev. 81, 925–939.
Chang, Y.F., Liu, X.G., 1983. Layer control type skarn type deposit—some deposits in the Middle-Lower Yangtze Depression in Anhui Province as an example. Miner. Depos. 2 (1), 11–20 (in Chinese).
Chang, Y.F., Liu, X.P., Wu, Y.Z., 1991. Metallogenic Belt of the Middle-Lower Yangtze River. Geological Publishing House, Beijing. 1-379 (in Chinese).
Cheng, H., Zhang, C., Vervoort, J.D., Lu, H.H., Wang, C., Cao, D.D., 2012. Zircon U-Pb and garnet Lu-Hf geochronology of eclogites from the Lhasa Block, Tibet. Lithos 155, 341–359.
Crowe, D.E., Riciputi, L.R., Bezenek, S., Ignatiev, A., 2001. Oxygen isotope and trace element zoning in hydrothermal garnets: windows into large-scale fluid flow behavior. Geology 29, 479–482.
Dai, R.R., Liu, C.G., 1984. The manner of occurrence and law of distribution of gold in the Xinqiao copper-sulfur-iron deposit. Geol. Rev. 30 (2), 126–134 (in Chinese with English abstract).
Doyle, M.G., Allen, R.L., 2003. Subseafloor replacement in volcanic-hosted massive sulfide deposits. Ore Geol. Rev. 23 (3), 183–222.
Du, Y.L., Deng, J., Cao, Y., Li, D.D., 2015. Petrology and geochemistry of Silurian-Triassic sedimentary rocks in the Tongling region of Eastern China: their roles in the genesis of large stratabound skarn ore deposits. Ore Geol. Rev. 67, 255–263.
Dziggel, A., Wulff, K., Kolb, J., Meyer, F.M., Lahaye, Y., 2009. Oscillatory zoning in metamorphic minerals: an indicator of infiltration metasomatism. Chem. Geol. 262, 262–276.
Einaudi, M.T., Burt, D.M., 1982. Introduction-terminology, classification, and composition of skarn deposits. Econ. Geol. 77 (4), 745–754.
Einaudi, M.T., Meinert, L.D., Newberry, R.J., 1981, Skarn deposits. Economic Geology. 75th Anniversary Volume, 317–391.
Fernando, G., Hauzenberger, C.A., Baumgartner, L.P., Hofmeister, W., 2003. Modeling of retrograde diffusion zoning in garnet: evidence for slow cooling of granulites from the Highland Complex of Sri Lanka. Mineral. Petrol. 78, 53–71.
Flynn, R.T., Burnham, W., 1978. An experimental determination of rare earth partition coefficients between a chloride containing vapor phase and silicate melts. Geochim. Cosmochim. Acta 42, 685–701.
Fu, S.G., Yan, X.Y., Yuan, C.X., 1977. Geologic feature of submarine volcanic eruption-sedimentary pyrite type deposit in Carboniferous in the Middle-Lower Yangtze River Valley metallogenic belt, Eastern China. J. Nanjing Univ.: Nat. Sci. Ed. 4, 43–67 (in Chinese).
Gaspar, M., 2005. The Crown Jewel gold skarn deposit. Ph.D. Thesis, Washington State University. Available from: http://griffin.wsu.edu/.
Gaspar, M., Knaack, C., Meinert, L.D., Moretti, R., 2008. REE in skarn systems: a LA–ICP-MS study of garnets from the Crown Jewel gold deposit. Geochim. Cosmochim. Acta 72, 185–205.
Gemmell, J.B., Zantop, H., Meinert, L.D., 1992. Genesis of the Aguilar zinc-lead-silver deposit, Argentina; contact metasomatic vs. sedimentary exhalative. Econ. Geol. 87 (8), 2085–2112.
Goodfellow, W., Lydon, J., Turner, R., 1993. Geology and genesis of stratiform sediment-hosted (SEDEX) zinc-lead-silver sulphide deposits. Geol. Assoc. Can. Spec. Pap. 40, 201–251.

Graham, S., Pearson, N., Jackson, S., Griffin, W., O'Reilly, S.Y., 2004. Tracing Cu and Fe from source to porphyry: in situ determination of Cu and Fe isotope ratios in sulfides from the Grasberg Cu–Au deposit. Chem. Geol. 207, 147–169.
Gu, L.X., Hu, W.X., He, J.X., 2000. Regional variations in ore composition and fluid features of massive sulfide deposits in South China: implications for genetic modeling. Episodes 23 (2), 110–118.
Gu, L.X., Xu, K.Q., 1986. On the carboniferous submarine massive sulfide deposit in the lower reaches of the Yangtze River. Acta Geol. Sin. 60 (2), 176–188 (in Chinese).
Guo, W.M., Lu, J.J., Jiang, S.Y., Zhang, R.Q., Qi, L., 2011. Re-Os isotope dating of pyrite from the footwall mineralization zone of the Xinqiao deposit, Tongling, Anhui Province: geochronological evidence for submarine exhalative sedimentation. Chin. Sci. Bull. 56 (36), 3860–3865 (in Chinese with English abstract).
Hong, W., Zhang, Z.H., Jiang, Z.S., Li, F.M., Liu, X.Z., 2012. Magnetite and garnet trace element characteristics from the Chagangnuoer iron deposit in the western Tianshan Mountains, Xinjiang, NW China: constrain for ore genesis. Acta Petrol. Sinica 28 (7), 2089–2102 (in Chinese with English abstract).
Huang, Z.C., 1999. Do there exist sea-floor volcanic eruptive sedements in the Huanglong Formation, Tongling Xinqiao area, Anhui Province. Geol. J. China Univ. 5, 110–112 (in Chinese with English abstract).
Huang, G.H., 2011. Mineralization characteristics and genesis of Xinqiao Cu-S-Au polymetallic deposit, Tongling, Anhui Province, China. Master Thesis, China University of Geosciences, Wuhan (in Chinese with English abstract).
Huang, S.S., Xu, Z.W., Ni, P., 2003. Inclusion geochemistry of Dongguashan hydrothermal superimposion copper deposit in the Tongling area, Anhui, China. Contrib. Geol. Miner. Resour. Res. 18 (1), 34–38 (in Chinese with English abstract).
Jamtveit, B., Wogelius, R.A., Fraser, D.G., 1993. Zonation patterns of skarn garnets: records of hydrothermal system evolution. Geology 21, 113–116.
Karimzadeh, S.A., 2010. Garnetization as a ground preparation process for copper mineralization: evidence from the Mazraeh skarn deposit, Iran. Int. J. Earth Sci. 99 (2), 343–356.
Kim, H.S., 2006. Deformation-induced garnet zoning. Gondwana Res. 10, 379–388.
Kravchuk, I.F., Ivanova, G.F., Varezhkina, N.S., Malinin, S.D., 1995. REE fractionation in acid fluid-magma systems. Geochem. Int. 32, 60–68.
Lai, J.Q., Chi, G.X., 2007. CO_2-rich fluid inclusions with chalcopyrite daughter mineral from the Fenghuangshan Cu–Fe–Au deposit, China: implications for metal transport in vapor. Miner. Deposita 42, 293–299.
Large, D.E., 1983. Sediment-hosted massive sulfide lead-zinc deposits: an empirical model. Mineral. Assoc. Canada Short Course Handb. 8, 1–30.
Leach, D.L., Sangster, D.F., Kelley, K.F., Large, R.R., Garven, G., Allen, C.R., Gutzmer, J., Walters, S., 2005. Sediment-hosted lead-zinc deposits: a global perspective. Econ. Geol. 100, 561–607.
Li, S., Yang, X.Y., Huang, Y., Sun, W.D., 2014. Petrogenesis and mineralization of the Fenghuangshan skarn Cu–Au deposit, Tongling ore cluster field, Lower Yangtze metallogenic belt. Ore Geol. Rev. 58, 148–162.
Ling, M.X., Wang, F.Y., Ding, X., Hu, Y.H., Zhou, J.B., Zartman, R.E., Yang, X.Y., 2009. Cretaceous rifge subduction along the Lower Yangtze River Belt, Eastern China. Econ. Geol. 104, 303–321.
Ling, Q.C., Cheng, H.L., 1998. Discussion on forming process and geological characteristics of magmatic skarn in Tongling area, Anhui Province. J. Changchun Univ. Sci. Technol. 28 (4), 366–371 (in Chinese with English abstract).
Liu, X.B., 2002. Geological characteristics and ore-controlling factor analysis of Xinqiao S-Fe deposit. Express Inf. Min. Ind. 22, 13–15 (in Chinese).
Liu, W.C., Gao, D.Z., Chu, G.Z., 1996. Aanalysis of tectonic deformation and metallogenic prediction in Tongling region. Geological Publishing House, Beijing, pp. 1–131 (in Chinese).
Liu, Y.S., Gao, S., Hu, Z.C., Gao, C.G., Zong, K.Q., Wang, D.B., 2010. Continental and oceanic crust recycling-induced melt-peridotite interactions in the Trans-North China Orogen: U-Pb dating, Hf isotopes and trace elements in zircons of mantle xenoliths. J. Petrol. 51, 537–571.
Mao, J.W., Shao, Y.J., Xie, G.Q., Zhang, J.D., Chen, Y.C., 2009. Mineral deposit model for porphyry-skarn polymetallic copper deposits in Tongling ore dense district of Middle-Lower Yangtze Valley metallogenic belt. Miner. Depos. 28 (2), 109–119 (in Chinese with English abstract).
Mao, J.W., Xie, G.Q., Duan, C., Franco, P., Dazio, I., Chen, Y.C., 2011. A tectono-genetic model for porphyry-skarn-stratabound Cu-Au-Fe and magnetite-apatite deposit along the Middle-Lower Yangtze River Valley, Eastern China. Ore Geol. Rev. 43 (1), 294–314.
Mao, J.W., Cheng, Y.B., Chen, M.H., Pirajno, F., 2013. Major types and time-space distribution of Mesozoic ore deposits in South China and their geodynamic settings. Miner. Depos. 48, 267–294.
Martin, L.A.J., Ballèvre, M., Boulvais, P., Halfpenny, A., Vanderhaeghe, O., Duchêne, S., Deloule, E., 2011. Garnet re-equilibration by coupled dissolution-reprecipitation: evidence from textural, major element and oxygen isotope zoning of 'cloudy' garnet. J. Metamorph. Geol. 29, 21–231.
Mayanovic, R.A., Anderson, A.J., Bassett, W.A., Chou, I.M., 2007. On the formation and structure of rare-earth element complexes in aqueous solutions under hydrothermal conditions with new data on gadolinium aquo and chloro complexes. Chem. Geol. 239, 266–283.
Mayanovic, R.A., Jayanetti, S., Anderson, A.J., Bassett, W.A., Chou, I.M., 2002. The structure of Yb3+ aquo ion and chloro complexes in aqueous solutions at up to 500 °C and 270 MPa. J. Phys. Chem. A 106, 6591–6599.
Meinert, L.D., 1992. Skarns and skarn deposits. Geosci. Can. 19, 145–162.
Meinert, L.D., 1997. Application of skarn deposit zonation models to mineral exploration. Explor. Min. Geol. 6, 185–208.
Meinert, L.D., Dipple, G.M., Nicolescu, S., 2005. World Skarn Deposits. Economic Geology, 100th Anniversary Volume, 299–336.
Meng, L.Y., 1994. Invasive type massive sulfide deposits in the Eastern China. Sci. China Ser. D 24 (1), 76–80 (in Chinese).
Meng, L.Y., 1996. Stable isotopes compositions characteristics of invasive type massive sulfide deposits. Chin. Sci. Bull. 41 (9), 808–810 (in Chinese).
Nakano, T., Takahara, H., Norimasa, N., 1989. Intracrystalline distribution of major elements in zoned garnet from skarn in the Chichibu mine, central Japan; illustration by color-coded maps. Can. Mineral. 27, 499–507.
Pan, Y., Done, P., 1999. The lower Changjiang (Yangtzi/Yangtze River) metallogenic belt, east-center China: intrusion and wall rock hosted Cu-Fe-Au, Mo, Zn, Pb, Ag deposits. Ore Geol. Rev. 15 (4), 177–242.
Pertermann, M., Hirschmann, M.M., Hametner, K., Günther, D., Schmidt, M.W., 2004. Experimental determination of trace element partitioning between garnet and silica-rich liquid during anhydrous partial melting of MORB-like eclogite. Geochem. Geophys. Geosyst. 5, Q05A01.
Qi, J.Z., Liu, H.Y., Jiang, Y.H., 2000. Yanshanian subduction and strike-sliping regime of East China, and its control of ore localization. Volcanol. Miner. Resour. 21 (4), 244–266 (in Chinese with English abstract).
Ravizza, G., Martin, C.E., German, C.R., Thompson, G., 1996. Os isotopes as tracers in seafloor hydrothermal system: metalliferous deposits from the TAG hydrothermal area, 26°N Mid-Atlantic Ridge. Earth Plant. Sci. Lett. 138, 105–119.
Reed, M.J., Candela, P.A., Piccoli, P.M., 2000. The distribution of rare earth elements between monzogranitic melt and the aqueous volatile phase in experimental investigations at 800 °C and 200 MPa. Contrib. Mineral. Petrol. 140, 251–262.
Sangster, D.F., 1990. Mississippi Valley-type and SEDEX lead-zinc deposits—a comparative examination. Institution of Mining and Metallurgy Trans-actions, Section B, Appl. Earth Sci. 99, 21–42.
Scherer, E.E., Cameron, K.L., Blichert-Toft, J., 2000. Lu-Hf garnet geochronology: closure temperature relative to the Sm-Nd system and the effects of trace mineral inclusions. Geochim. Cosmochim. Acta 64, 3413–3432.
Schmidt, A., Mezger, K., O'Brien, P.J., 2011. The time of eclogite formation in the ultrahigh pressure rocks of the Sulu terrane: constraints from Lu–Hf garnet geochronology. Lithos 125, 743–756.
Shannon, R.D., 1976. Revised effective ionic radii and systematic studies of interatomic distances in halides and chalcogenides. Acta Crystallogr. Section A, Crystal Phys. Diffr. Theor. General Crystallogr. 32, 751–767.
Smith, M.P., Henderson, P., Jeffries, T.E.R., Long, J., Williams, C.T., 2004. The rare earth elements and uranium in garnets from the Beinn and Dubhaich Aureole, Skye, Scotland, UK: constraints on processes in a dynamic hydrothermal system. J. Petrol. 45, 457–484.
Somarin, A.K., 2004. Garnet composition as an indicator of Cu mineralization: evidence from skarn deposits of NW Iran. J. Geochem. Explor. 81, 47–57.
Sun, S., McDonough, W.F., 1989. Chemical and isotopic systematics of oceanic basalts: implications for mantle composition and processes. In: Saunders, A.D., Norry, M.J. (Eds.), Magmatism in the Ocean Basins, 42. Geological Society of London Special Publication, pp. 313–345.
Sverjensky, D.M., 1984. Europium redox equilibria in aqueous solution. Earth Planet. Sci. Lett. 67, 70–78.
Tang, Y.C., Wu, Y.Z., Cu, G.Z., Xing, F.M., Wang, Y.M., Cao, F.Y., Chang, Y.F., 1998. Copper gold polymetallic ore deposit geology in the region along Yangtze River in Anhui Province. Geological Publishing House, Beijing. 1-351 (in Chinese).
Vander, A.J., Andre, L., 1991. Trace elements (REE) and isotopes (O, C, Sr) to characterize the metasomatic fluid sources: Evidence from the skarn deposit (Fe, W, Cu) of Traversella (Ivrea, Italy). Contrib. Miner. Petrol. 106 (3), 325–339.
Wang, Y., Zhu, X.K., Cheng, Y.B., 2013. Ore microscopy & Fe isotope of the Xinqiao deposit and their constraints on the ore genesis. J. Jilin Univ.: Earth Sci. Ed. 43 (6), 1787–1798 (in Chinese with English abstract).
Wang, Y., Zhu, X.L., Mao, J.W., Li, Z.H., Cheng, Y.B., 2011. Iron isotope fractionation during skarn-type metallogeny: a case study of Xinqiao Cu-S-Fe-Au Deposit in the Middle-Lower Yangtze Valley. Ore Geol. Rev. 43, 194–202.
Wang, Y.B., Liu, D.Y., Meng, Y.F., Zeng, P.S., Yang, Z.S., Tian, S.A., 2004. SHRIMP U-Pb geochronology of the Xinqiao Cu-S-Fe-Au deposit in the Tongling ore district, Anhui, China. Geol. China 31 (2), 169–173 (in Chinese with English abstract).
Wang, S.W., Zhou, T.F., Yuan, F., Fan, Y., Zhang, L.J., Song, Y.L., 2015. Petrogenesis of Dongguashan skarn-porphyry Cu-Au deposit related intrusion in the Tongling district, eastern China: geochronological, mineralogical, geochemical and Hf isotopic evidence. Ore Geol. Rev. 64, 53–70.
Wu, F.Y., Ge, W.C., Sun, D.Y., Guo, C.L., 2003. Discussions on the lithospheric thinning in Eastern China. Earth Sci. Front. 10 (3), 51–60 (in Chinese with English abstract).
Wu, C.L., Dong, S.W., Robinson, P.T., Frost, B.R., Gao, Y.H., Lei, M., Chen, Q.L., Qin, H.P., 2014. Petrogenesis of high-K, calc-alkaline and shoshonitic intrusive rocks in the Tongling area, Anhui Province (eastern China), and their tectonic implications. Geol. Soc. Am. Bull. 126, 78–102.
Xiao, C.D., Liu, X.W., 2002. REE geochemistry and origin of skarn garnets from eastern Inner Mongolia. Geol. China 29 (3), 311–316 (in Chinese with English abstract).
Xie, H.G., Wang, W.B., Li, W.D., 1995. The genesis and metallogenetic of Xinqiao Cu-S-Fe deposit, Anhui Province. Volcanol. Miner. Resour. 16 (2), 101–107 (in Chinese with English abstract).

Xu, G., Zhou, J., 2001. The Xinqiao Cu-S-Fe-Au deposit in the Tongling mineral district, China: synorogenetic remobilization of a stratiform sulfide deposit. Ore Geol. Rev. 18, 77–94.

Xu, K.Q., Zhu, J.C., 1978. Genesis discussion about sedimentary (or volcanic sedimentary) and reworked by hydrothermal copper deposits in several fault depression belts in Southeast China. Geol. Inform. Fujian 4, 1–110 (in Chinese).

Xu, W.Y., Yang, Z.S., Meng, Y.F., Zeng, P.S., Shi, D.N., Tian, S.H., Li, H.Y., 2004. Genetic Model and Dynamic Migration of Ore-forming Fluids in Carboniferous Exhalation-Sedimentary Massive Sulfide Deposits in Tongling District, Anhui Province. Miner. Deposits 23 (3), 353–364 (in Chinese with English abstract).

Yang, D.F., Fu, D.X., Wu, N.X., 1982. Genesis of pyrite type copper in Xinqiao and its neighboring region according to ore composition and structure. Issue of Nanjing Institute of Geology and Mineral Resources, Chinese Academy of Geological Sciences 3 (4), 59–68 (in Chinese with English abstract).

Yardley, B.W., Rochelle, C.A., Barnicoat, A.C., Lloyd, G.E., 1991. Oscillatory zoning in metamorphic minerals: an indicator of infiltration metasomatism. Mineral. Mag. 55, 357–365.

Ying, L.J., Tang, J.X., Wang, D.H., Wang, W.P., 2012. Features of garnet in the Jiama super-large Cu polymetallic deposit and its genetic significance. Acta Geol. Sinica 86 (11), 1735–1747 (in Chinese with English abstract).

Zang, W.S., Wu, G.G., Zhang, D., Liu, A.H., 2004. Geological and geochemical characteristics and genetic analyses of Xinqiao Iron Orefield, Tongling. Geotectonica et Metallogenia 28 (2), 187–193 (in Chinese with English abstract).

Zhai, D.G., Liu, J.J., Zhang, H.Y., Wang, J.P., Su, L., Yang, X.A., Wu, S.H., 2014. Origin of oscillatory zoned garnets from the Xieertala Fe–Zn skarn deposit, northern China: in-situ LA–ICP-MS evidence. Lithos 190–191, 279–291.

Zhai, Y.S., Yao, S.Z., Lin, X.D., Jin, F.Q., Zhou, X.R., Wan, T.F., Zhou, Z.G., 1992. Metallogenic regularity of iron and copper deposits in the Middle-Lower valley of the Yangtze River. Miner. Depos. 11 (1), 1–235 (in Chinese with English abstract).

Zhang, Y., 2015. Genesis of Xinqiao Cu-S-Fe deposit, Tongling, Anhui Province, China. Ph. D. Dissertation. Central South University (in Chinese with English abstract).

Zhang, Y., Shao, Y.J., Chen, H.Y., Liu, Z.F., Li, D.F., 2016. A hydrothermal origin for the large Xinqiao Cu-S-Fe deposit, Eastern China: Evidence from sulfide geochemistry and sulfur isotopes. Ore Geol. Rev. http://dx.doi.org/10.1016/j.oregeorev.2016.08.002.

Zhang, Y., Shao, Y.J., Li, H.B., Liu, Z.F., 2017. Genesis of the Xinqiao Cu–S–Fe–Au deposit in the Middle-Lower Yangtze River Valley metallogenic belt, Eastern China: constraints from U-Pb–Hf, Rb–Sr, S, and Pb isotopes. Ore Geol. Rev. 86, 100–116.

Zhao, B., Zhao, J.S., Liu, H.C., 1999. REE geochemical studies of whole rock and rock-forming minerals in skarns from Cu (Au), Cu-Fe (Au) and Fe ore deposits distributed along Middle-Lower Reaches of Yangtze River, China. Geochimica 28 (2), 113–125 (in Chinese with English abstract).

Zhao, J.S., Qiu, X.L., Zhao, B., Tu, X.L., Yu, Q., Lu, T.S., 2007. REE geochemistry of mineralized skarns from Daye to Wushan region, China. Geochimica 36 (4), 400–412 (in Chinese with English abstract).

Zheng, Z., Du, Y.S., Cao, Y., Cao, Z.W., Yang, S., Dong, Q., 2012. The composition characteristics and origin of garnets in the Dongguashan skarn copper deposit, Anhui Province, China. Acta Petrol. Mineral. 31 (2), 235–242 (in Chinese with English abstract).

Zhou, T.F., Zhang, L.J., Yuan, F., Fang, Y., Cooke, D.R., 2010. LA-ICP-MS in situ trace element analysis of pyrite from the Xinqiao Cu-Au-S Deposit in Tongling, Anhui, and its constrains on the ore genesis. Earth Sci. Front. 17 (2), 306–319 (in Chinese with English abstract).